Ab Initio and DFT Direct Dynamics Studies on the Reaction Path and Rate Constant of the Hydrogen Abstraction Reaction: $SiH_3F + H \rightarrow SiH_2F + H_2$

Shen-Min Li,*,† Xin Yu,† Zhen-Feng Xu,‡ Ze-Sheng Li,† and Chia-Chung Sun†

Institute of Theoretical Chemistry, State Key Laboratory of Theoretical and Computational Chemistry, Jilin University, Changchun 130023, People's Republic of China, and Department of Applied Chemistry, Beijing University of Chemical Technology, Beijing 100029, People's Republic of China

Received: September 25, 2000; In Final Form: December 27, 2000

Ab initio and density functional theory (DFT) direct dynamics methods have been used to study the title reaction, and the results of the two methods have been fully compared. First, electronic structure information, including geometries, gradients, and force constants (Hessians), are calculated using ab initio UQCISD and DFT BHLYP methods with the 6-311+G** basis set. Furthermore, the energies of some selected points along the minimum-energy path (MEP) are improved by a series of single-point G2//QCISD and PMP4/6-311+G(3df,2p)//BHLYP calculations. Then, the changes of the geometries, generalized normal-mode vibratioanal frequencies, potential energies, and total curvature along the MEP of the two methods are discussed and compared. Finally, the reaction rate constants within 200−3000 K are calculated by canonical variational transition-state theory with the small-curvature tunneling correction (CVT/SCT) method. The results show that the DFT method is good enough in comparison with the ab initio method for the reaction to obtain satisfactory reaction rate constants. The variational effect is small, and in the lower-temperature range, the small-curvature tunneling effect is important for the reaction. Fluorine substitution decreases the reactivity of the Si−H bond toward H atom attack, and the decrease in k/n mainly stems from a corresponding increase in activation energy. The reaction rate constant based on the scaled PMP4/6-311+G(3df,2p)//BHLYP potential energy curve is in the excellent agreement with the experimental value at 293 K, and the rate constants within 200−3000 K are fitted to be a three-parameter expression: $k = 3.3 \times 10^5 T^{2.60} \exp(-737/T)$ cm^3 mol^{-1} s^{-1}.

Introduction

Previously, the dynamic properties and theoretical rate constants of the reactions of H atoms with silane and chlorosilane have attracted our interest significantly,[1,2] and the effect of chlorine substitution on the reaction reactivity trend has been studied. As part of our ongoing work in this field, this paper investigates theoretically the dynamic properties of the reaction of $SiH_3F + H \rightarrow SiH_2F + H_2$. In recent years, fluorosilanes have drawn considerable attention because of their importance in the semiconductor industry.[3−5] The thermochemical properties of fluorosilanes are also the subject of some theoretical studies.[6,7] Reactions of H atoms, the simplest free radical species, are of particular interest since these reactions provide an uncomplicated probe of chemical reactivity. In the most recent work in experiment, Koshi Mitsuo et al.[8] made a study of the reaction of $SiH_3F + H \rightarrow SiH_2F + H_2$ and gave the reaction rate constant at room temperature. No other kinetic data is available for the reaction, and to our knowledge, little theoretical attention has been paid to this reaction.

In this paper, ab initio direct dynamic method[9] and DFT direct dynamic method[10] are applied to study the title reaction. The origin of the selection of two methods is that the recent work of us indicates that G2//QCISD method is applicable to study the reactions of H atoms with silane and chlorosilane. Because of the similarity of fluorosilane to chlorosilane, it is expected that the G2//QCISD method should still be appropriate in studying this reaction. On the other hand, with the increasing of molecular size, the calculation resource that the UQCISD method needs is very large and even intolerable. Therefore, it is essential to search a new method to obtain the same accuracy but to spend much less calculation resource. It has been showed earlier by Truong et al.[11−14] that the combination of Becke's half-and-half (BH) with Lee−Yang−Parr (LYP) correlation functionals can be used effectively to calculate the geometries and Hessians along the MEP particularly for open-shell systems. In the present study, the BHLYP method and the 6-311+G** basis set are adopted to determine structure, force, and Hessian information. Considering the energies of the MEP constructed by DFT method is not always sufficiently accurate for rate-constant calculation, so spin-projected fourth-order Moller−Plesset perturbation theory (PMP4) is performed using a larger 6-311+G(3df,2p) basic set to obtain more accurate information on the energy, and the results are compared with those of the G2//QCISD method.

Calculation Methods

By means of the GAUSSIAN 98 program,[15] high-level ab initio and DFT calculations are carried out. First, the geometries and frequencies of the stationary points (reactant, transition state, and products) are calculated at the UQCISD/6-311+ G** and

* Corresponding author. FAX: +86−431−8945942. E-mail:shenmin@public.cc.jl.cn.

† Jilin University, Changchun 130023.

‡ Beijing University of Chemical Technology.

10.1021/jp003460n CCC: $20.00
Published on Web 04/03/2001

TABLE 1: Geometrical Parameters (distances in Å and angles in deg) of the Equilibrium and Transition-State Structures at the UQCISD/6-311+G and BHLYP/6-311+G** Levels**

	geometrical parameters	UQCISD/6-311+G**	BHLYP/6-311+G**	previous calc.[a]	exptl[b]
SiH_3F (C_{3v})	r_{SiH}	1.4709	1.4690	1.478	1.484
	r_{SiF}	1.6210	1.6125	1.635	1.593
	∠HSiH	110.8955	110.9946		110.63
	∠HSiF	108.0064	107.9011	109.2	108.4
SiH_2F (Cs)	r_{SiH}	1.4771	1.4769	1.483	
	r_{SiF}	1.6255	1.6163	1.640	
	∠HSiH	111.7713	111.8957	110.7	
	∠HSiF	107.7993	107.5584	109.9	
H_2	r_{HH}	0.7436	0.7383		0.7414
TS					
$SiH_2F-H'-H''$ (Cs)	$r_{H'H''}$	1.0750	1.1157		
	$r_{SiH'}$	1.6262	1.6023		
	r_{SiH}	1.4737	1.4713		
	r_{SiF}	1.6212	1.6118		
	∠H″H′Si	180.	180.		
	∠HSiH′	110.3667	110.4232		
	∠FSiH′	107.7889	107.8185		
	∠HSiH	111.7135	111.7856		
	∠HSiF	108.2375	108.1256		

[a] Ref 6. [b] Ref 21.

TABLE 2: Harmonic Vibrational Frequencies (cm^{-1}) of the Equilibrium and Transition-State Structures at the UQCISD/6-311+G and BHLYP/6-311+G** levels**

	UQCISD/6-311+G**	BHLYP/6-311+G**	previous calc.[a]	exptl[b]
SiH_3F	(*E*)743 (*A1*)861	(*E*)747 (*A1*)874	(*E*)800(*A1*)943	(*E*)728 (*A1*)872
	(*E*)999 (*A1*)1027	(*E*)1002 (*A1*)1029	(*E*)990(*A1*)1132	(*E*)956 (*A1*)990
	(*E*)2331 (*A1*)2326	(*E*)2337 (*A1*)2334	(*E*)2338(*A1*)2352	(*E*)2196 (*A1*)2206
SiH_2F	(*A*″)726(*A*′)824	(*A*″)729 (*A*′)824	(*A*″)775 (*A*′)863	
	(*A*′)862(A′)960	(*A*′)872(A′)960	(*A*′)935 (*A*′)1005	
	(*A*′)2261(*A*″)2295	(*A*′)2255 (*A*″)2293	(*A*′)2293 (*A*″)2312	
H_2	(Σ_g^+) 4419	(Σ_g^+) 4519	(Σ_g^+ 4403)	
TS	(*A*′)177(A″)304	(*A*′)184(A″)309		
	(*A*″)733 (*A*′)810	(*A*″)740 (*A*′)811		
	(*A*′)858 (*A*′)965	(*A*′)873 (*A*′)974		
	(*A*″)1048 (*A*′)1057	(*A*″)1037 (*A*′)1053		
	(*A*′)1125 (*A*′)2299	(*A*′)1162 (*A*′)2309		
	(*A*″)2317 (*A*′)1502*i*	(A″)2325 (*A*′)1200*i*		

[a] Ref 6. [b] Ref 22.

BHLYP/6-311+G** levels. Then, the MEP at each level is obtained from $s = -0.2$ to 0.2 $(amu)^{1/2}$ bohr by intrinsic reaction coordinate (IRC) theory in mass-weighed Cartesian coordinates. The gradient step size is 0.05 $(amu)^{1/2}$ bohr at the UQCISD/6-311+G** level and 0.02 $(amu)^{1/2}$ bohr at the BHLYP/6-311+G** level. To obtain accurate reaction rate constant, we refined the energies of some selected points along the MEP at the G2//QCISD and PMP4/6-311+G(3df,2p)//BHLYP levels, respectively. The G2//QCISD method[16] applies the G2 method[17] at the UQCISD stationary point geometries and along the UQCISD MEP. Finally, the harmonic vibrational frequencies as well as the force-constant matrixes of the selected points near the transition state are calculated.

To obtain the theoretical rate constants and temperature dependence, we performed the POLYRATE-Version 8.4.1 program.[18] The Euler-with-stabilization integrator with a step size of 0.0001 $(amu)^{1/2}$ bohr is used to follow the MEP, and the generalized normal-mode analysis is performed every 0.01 $(amu)^{1/2}$ bohr. The curvature components are calculated using a quadratic fit to obtain the derivative of the gradient with respect to the reaction coordinate. Canonical variational transition-state theory rate constants are calculated with the small-curvature tunneling correction method proposed by Truhlar and co-workers,[19,20] since the heavy−light−heavy mass combination is not present in this hydrogen abstraction reaction.

Results and Discussion

A. Stationary Points. The optimized geometric parameters and harmonic vibrational frequencies of the reactant (SiH_3F), products (SiH_2F and H_2), and transition state ($SiH_2F-H'-H''$) at the UQCISD/6-311+G** and BHLYP/6-311+G** levels are given in Tables 1 and 2. It is easy to see that the difference of the optimized geometric parameters and harmonic vibrational frequencies of the reactant and products at the two levels is small. When comparison is possible, both of the results are in good agreement with the experimental values,[21,22] and the maximum error of the freaquencies is about 6%. Schlegel[6] also calculated the geometries and frequencies of SiH_3F and SiH_2F at the HF/3-21G level, and he obtained similar results. It implies that for the reactant (SiH_3F) and the product (SiH_2F), the calculated geometries and frequencies are insensitive to the applied calculated methods and basis sets.

For the transition state, the optimized geometric parameters and harmonic vibrational frequencies calculated at the BHLYP/6-311+G** level are in good agreement with the values calculated at the UQCISD/6-311+G** level, except for the value of the imaginary frequency (1200 versus 1502 cm^{-1}). The geometric parameters show that the transition-state structure is reactant-like, and the hydrogen abstraction reaction will proceed via an early transition state. For example, at the BHLYP/6-

TABLE 3: Reaction Enthalpies (ΔH^0_{298}) and Potential Barriers (ΔE) (kcal/mol)[a]

	UQCISD	G2//QCISD	BHLYP	PMP4//BHLYP	exptl
ΔH^0_{298}	−9.78	−9.98	−10.49	−9.69	−10.31
ΔE	7.57	6.58	3.46	6.07	

[a] Total energies (in hartrees) at UQCISD(ZPE): SiH_3F, −390.514214; H, −0.499810; SiH_2F, −389.872201; H_2, −1.158274; TS, −391.001961. At G2//QCISD: SiH_3F, −390.643825; H, −0.50; SiH_2F, −389.994326; H_2, −1.166254; TS, −391.133336. At BHLYP(ZPE): SiH_3F, −391.155806; H, −0.498546; SiH_2F, −390.512610; H_2, −1.159323; TS, −391.648839. At PMP4/6-311+G(3df,2p)//BHLYP: SiH_3F, −390.606699; H, −0.499810; SiH_2F, −389.962890; H_2, −1.159926; TS, −391.096828.

311+ G** level, the length of bond Si−H′, which will be broken, increases by 9% with respect to the Si−H equilibrium bond length of SiH_3F, while the length of the H′−H″ bond, which will form a hydrogen molecule, is 1.5 times as large as the equilibrium bond length of the hydrogen molecule.

Table 3 lists the reaction enthalpies and potential barriers calculated at the four different levels of UQCISD/6-311+G**, G2//QCISD, BHLYP/6-311+G**, and PMP4/6-311+G(3df,-2p)//BHLYP. At 298 K, the reaction enthalpies are −9.78, −9.98, −10.49, and −9.69 kcal/mol, respectively. As can be seen, the difference among the reaction enthalpies at the four levels is not obvious, and all of them are close to the corresponding experimental value of −10.31 kcal/mol derived from the experimental standard heats of formation (SiH_3F, −90.30 kal/mol;[23] SiH_2F, −48.49 kcal/mol (estimated by linear interpolation);[6] H, 52.12 kcal/mol;[21] H_2, 0.0 kcal/mol). On the other hand, the potential barrier calculated at the BHLYP/6-311+G** level has a substantial difference from the values calculated at the other three levels. It is at least 2.5 kcal/mol less than the others. In comparison with the UQCISD/6-311+G** method, the G2//QCISD method decreases the reaction potential barrier height by about 1 kcal/mol, and PMP4/6-311+G(3df,2p)//BHLYP decreases by more than 1 kcal/mol.

In conclusion, we find that the UQCISD/6-311+G** and BHLYP/6-311+G** levels can provide accurate structural and frequency information, and additional G2//QCISD and PMP4/6-311+G(3df,2p)//BHLYP calculations are essential to improving the potential energy curve. In addition, the PMP4/6-311+G(3df,2p)//BHLYP method has an absolute advantage in calculation resource in comparison with the method of G2//QCISD.

B. Reaction Path Properties. The minimum-energy path is calculated at the UQCISD/6-311+G** and BHLYP/6-311+G** levels by the intrinsic reaction coordinate theory. The energies of some selected points on the MEP are refined by the G2//QCISD and PMP4/6-311+G(3df,2p)//BHLYP methods. At the PMP4/6-311+G(3df,2p)//BHLYP level, the position of the maximum value for the potential energy curve corresponds to the saddle-point position ($s = 0$) at the BHLYP/6-311+G** level, whereas at the G2//QCISD level, the maximum-value position is shifted slightly toward the reactants to approximately $s = -0.05$ (amu)$^{1/2}$ bohr. This kind of artificial shifting is caused by the computational technique, which can be reoriented by the RODS (reorient the dividing surface) algorithm in the POLYRATE-Version 8.4.1 program.

Figures 1a,b and 2a,b show the changes of the bond lengths and generalized normal-mode vibrational frequencies along the MEP as functions of intrinsic reaction coordinate s [(amu)$^{1/2}$ bohr] at the UQCISD/6-311+G** and BHLYP/6-311+G** levels, respectively. At the two levels, the changes of the bond lengths are very similar, and the similarity is found also in the

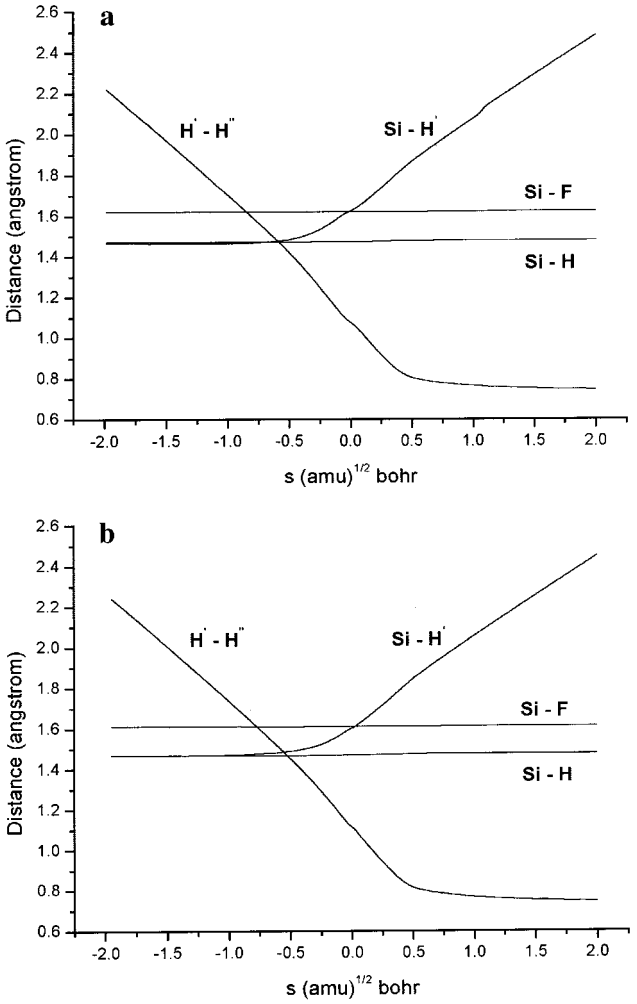

Figure 1. (a) Changes of the bond lengths (in ångströms) as functions of s [(amu)$^{1/2}$ bohr] at the UQCISD/6-311+G** level. (b) Same as those in panel a except at the BHLYP/6-311+G** level.

frequency changes. In Figure 1a,b, with the Si−H′ and H′−H″ bond lengths changing strongly in the course of the reaction, the other bond lengths keep no change. In Figure 2a,b, the solid line signifies that the harmonic Si−H′ stretching vibrational frequency, corresponding to the generalized normal mode that breaks during the reaction, drops dramatically near the saddle point, and this mode correlates with H′−H″ stretch at the product region. These behaviors are known to be the typical features of hydrogen abstraction reactions. In addition, from the changes of bond lengths and frequencies, it is found that the "reaction region" is in the range of $s = -0.5$ to 0.5 (amu)$^{1/2}$ bohr.

Figure 3 shows the classical potential energy, V_{MEP}, the zero-point energy, ZPE, and the ground-state vibrational adiabatic potential energy, V_a^G as functions of s [(amu)$^{1/2}$ bohr] at the G2//QCISD and PMP4/6-311+G(3df,2p)//BHLYP levels. Notice that the G2//QCISD potential energy curves (dashed lines) are similar to those of PMP4/6-311+G(3df,2p)//BHLYP (solid lines). At each level, the maximum positions of the V_{MEP} and V_a^G are the same, and the ZPE curve is practically constant as s varies with only a gentle fall near the saddle point ($s = 0$), which implies that the variational effect for the reaction will be small or almost negligible.

Figure 4 shows the changes of the total reaction path curvature as functions of s [(amu)$^{1/2}$ bohr] at the G2//QCISD and PMP4/6-311+G(3df,2p)//BHLYP levels. As can be seen, at each level there are two sharp peaks, one before and one after the saddle

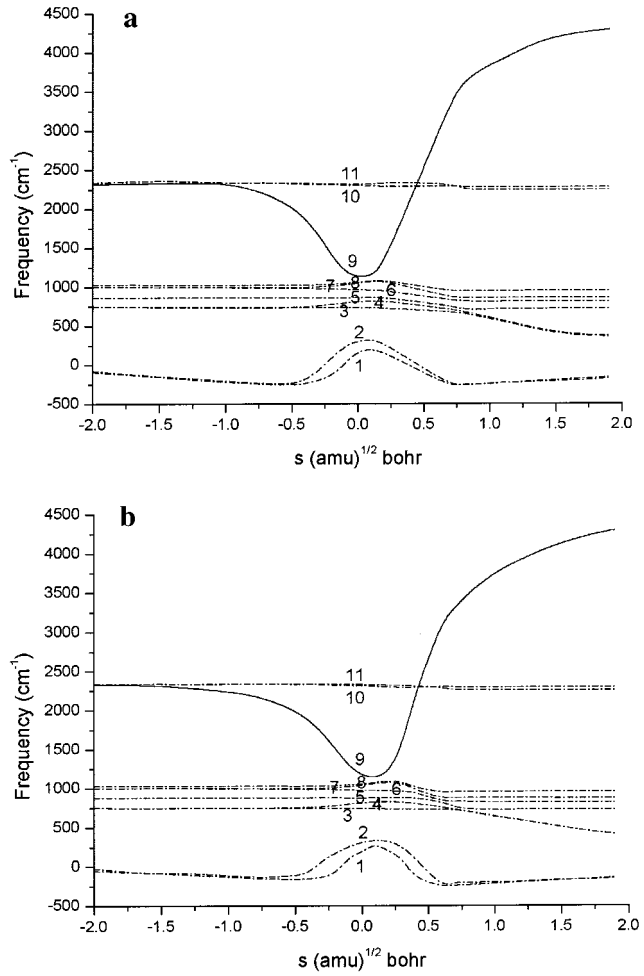

Figure 2. (a) Changes of the generalized normal-mode vibrational frequencies as functions of s [(amu)$^{1/2}$ bohr] at the UQCISD/6-311+G** level. (b) Same as those in panel a except at the BHLYP/6-311+G** level.

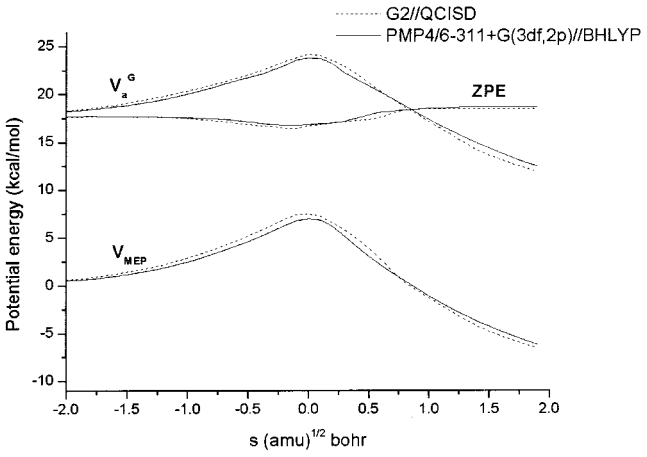

Figure 3. Classical potential energy (V_{MEP}), zero-point energy (ZPE), and ground-state vibrationally adiabatic potential energy (V_a^G) as functions of s [(amu)$^{1/2}$ bohr] at the G2//QCISD and PMP4/6-311+G(3df,2p)//BHLYP levels.

point, due to the strong couplings of the reaction coordinate with the Si−H′ and H′−H″ stretches, respectively. The total-curvature values of the two peaks are about 1.8 and 2.9 au, respectively, at the G2//QCISD level in comparison with 2.0 and 3.5 au, respectively, at the PMP4/6-311+G(3df,2p)//BHLYP level. It seems that at the PMP4/6-311+G(3df,2p)//BHLYP level, a slightly larger reaction-path curvature is obtained;

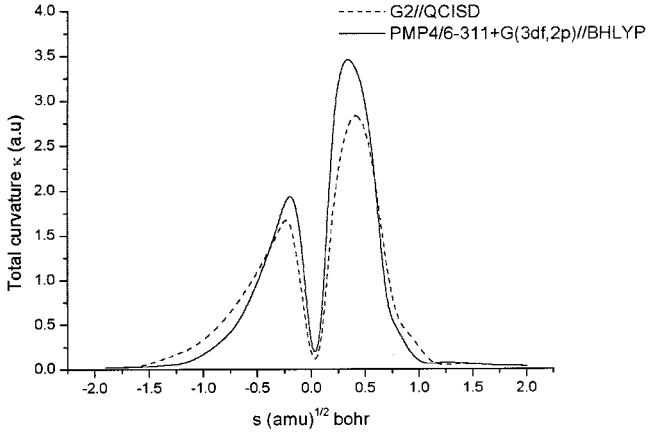

Figure 4. Changes of the total reaction-path curvature as functions of s [(amu)$^{1/2}$ bohr] at the G2//QCISD and PMP4/6-311+G(3df,2p)//BHLYP levels.

however, the curvature is not severe. Therefore, the SCT correction method for calculating the reaction rate constant should be suitable.

C. Rate Constant Calculation. The canonical variational transition-state theory rate constants with the small-curvature tunneling correction (CVT/SCT) for the reaction are calculated in a wide temperature range of 200−3000 K at the UQCISD/6-311+G**, G2//QCISD, BHLYP/6-311+G**, and PMP4/6-311+G(3df,2p)//BHLYP levels, and the results are listed in the second to the fifth columns of Table 4. For the purpose of comparison, both the conventional transition-state theory (TST) and the canonical variational transition-state theory (CVT) are applied to obtain the reaction rate constants within the same temperature range, and the results at the PMP4/6-311+G(3df,-2p)//BHLYP level are listed in the seventh and eighth columns of Table 4. We would like to emphasize three points about this Table. First, there is a very slight difference between the TST rate constants and CVT rate constants within the whole temperature range, which enables us to conclude that the variational effect is very small or almost negligible. Second, by comparing the CVT/SCT rate constants with those of CVT at the PMP4/6-311+G(3df,2p)//BHLYP level, it is not difficult to find that the small-curvature tunneling correction plays an important role within the lower temperature range. Third, at the experimentally measured temperature (293K), the experimental rate constant is 32.18, 4.98, 0.14, and 1.89 times as large as the CVT/SCT ones calculated at the UQCISD/6-311+G**, G2//QCISD, BHLYP/6-311+ G** and PMP4/6-311+G(3df,-2p)//BHLYP levels, respectively. It means that the CVT/SCT rate constant at the PMP4/6-311+G(3df,2p)//BHLYP level presents the best agreement with the experimental value,[8] and the G2//QCISD rate constant is in better agreement. While at the same temperature, the method of BHLYP/6-311+G** overestimates the reaction rate constant, and the method of UQCISD/6-311+G** underestimates it. Notice that even at the present PMP4/6-311+G(3df,2p)//BHLYP level, the rate constant is still underestimated. One important factor is that the potential barrier is overestimated at that level. To seek true potential barrier of this reaction, we performed a series of high-level single-point calculations at the PMP4/GTlarge//BHLYP, QCISD/cc-pVTZ//QCISD, QCISD/6-311+G(3df,2p)//QCISD, and QCISD/GTlarge//QCISD levels. The obtained potential barriers are 6.23, 6.29, 6.69, and 6.88 kcal/mol, respectively, and they are even higher than the PMP4/6-311+G(3df,2p)//BHLYP value, 6.07 kcal/mol. It implies that at these levels, the rate constant will be underestimated more. An alternative method

TABLE 4: Reaction Rate Constants ($cm^3\ mol^{-1}\ s^{-1}$) in the Temperature Range of 200−3000 K

	CVT/SCT					TST	CVT
T	UQCISD/ 6-311+G**	G2// QCISD	BHLYP/ 6-311+G**	PMP4/6-311+G (3df,2p)//BHLYP	PMP4/6-311+G(3df, 2p)//BHLYP(scaled)	PMP4/6-311+G (3df,2p)//BHLYP	PMP4/6-311+G (3df,2p)//BHLYP
200	1.35×10^8	1.19×10^9	1.07×10^{11}	4.01×10^9	8.73×10^9	8.49×10^6	7.83×10^6
293[a]	2.06×10^9	1.33×10^{10}	4.69×10^{11}	3.51×10^{10}	6.50×10^{10}	1.26×10^9	1.14×10^9
300	2.46×10^9	1.53×10^{10}	5.12×10^{11}	3.98×10^{10}	7.29×10^{10}	1.63×10^9	1.48×10^9
350	7.59×10^9	3.73×10^{10}	8.97×10^{11}	8.73×10^{10}	1.52×10^{11}	7.65×10^9	6.93×10^9
400	1.96×10^{10}	7.89×10^{10}	1.44×10^{12}	1.67×10^{11}	2.79×10^{11}	2.52×10^{10}	2.25×10^{10}
450	4.38×10^{10}	1.49×10^{11}	2.14×10^{12}	2.92×10^{11}	4.68×10^{11}	6.50×10^{10}	5.76×10^{10}
500	8.73×10^{10}	2.61×10^{11}	3.04×10^{12}	4.72×10^{11}	7.35×10^{11}	1.41×10^{11}	1.25×10^{11}
600	2.68×10^{11}	6.63×10^{11}	5.43×10^{12}	1.05×10^{12}	1.55×10^{12}	4.71×10^{11}	4.11×10^{11}
800	1.31×10^{12}	2.56×10^{12}	1.29×10^{13}	3.43×10^{12}	4.67×10^{12}	2.37×10^{12}	2.04×10^{12}
1000	3.90×10^{12}	6.63×10^{12}	2.42×10^{13}	8.01×10^{12}	1.04×10^{13}	6.87×10^{12}	5.81×10^{12}
1200	8.73×10^{12}	1.36×10^{13}	3.95×10^{13}	1.53×10^{13}	1.90×10^{13}	1.49×10^{13}	1.24×10^{13}
1400	1.63×10^{13}	2.39×10^{13}	5.86×10^{13}	2.56×10^{13}	3.10×10^{13}	2.70×10^{13}	2.22×10^{13}
1600	2.70×10^{13}	3.77×10^{13}	8.19×10^{13}	3.91×10^{13}	4.63×10^{13}	4.34×10^{13}	3.55×10^{13}
1800	4.10×10^{13}	5.52×10^{13}	1.09×10^{14}	5.59×10^{13}	6.50×10^{13}	6.44×10^{13}	5.22×10^{13}
2000	5.85×10^{13}	7.65×10^{13}	1.40×10^{14}	7.59×10^{13}	8.73×10^{13}	9.03×10^{13}	7.23×10^{13}
2200	7.95×10^{13}	1.02×10^{14}	1.73×10^{14}	9.94×10^{13}	1.13×10^{14}	1.20×10^{14}	9.58×10^{13}
2400	1.04×10^{14}	1.30×10^{14}	2.11×10^{14}	1.26×10^{14}	1.42×10^{14}	1.55×10^{14}	1.23×10^{14}
2600	1.33×10^{14}	1.63×10^{14}	2.52×10^{14}	1.57×10^{14}	1.75×10^{14}	1.93×10^{14}	1.53×10^{14}
2800	1.64×10^{14}	1.98×10^{14}	2.95×10^{14}	1.89×10^{14}	2.10×10^{14}	2.37×10^{14}	1.87×10^{14}
3000	1.99×10^{14}	2.38×10^{14}	3.42×10^{14}	2.25×10^{14}	2.48×10^{14}	2.84×10^{14}	2.23×10^{14}

[a] The value of the experimental rate constant at 293 K is 6.63×10^{10} $cm^3\ mol^{-1}\ s^{-1}$.

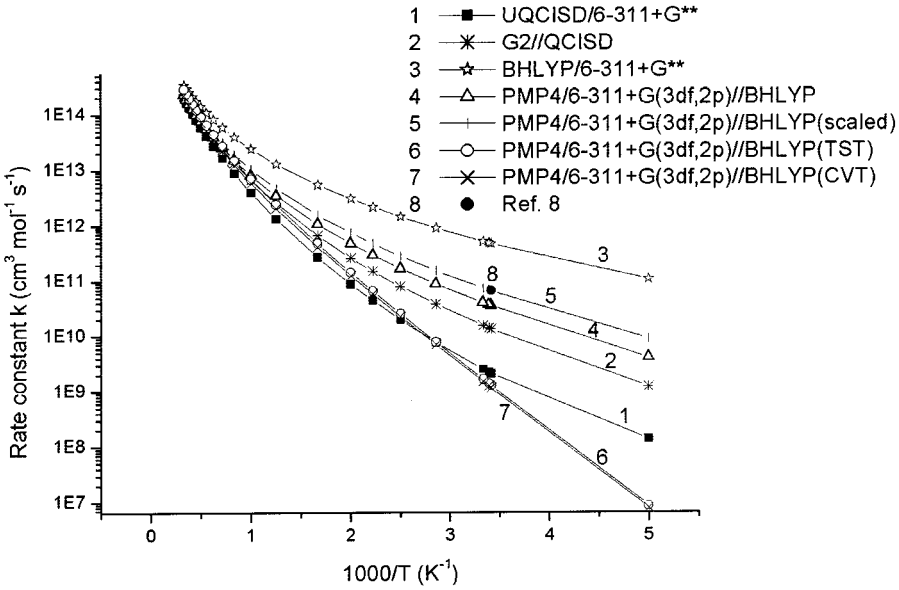

Figure 5. Plot of the CVT/SCT rate constants at the UQCISD/6-311+G**, G2//QCISD, BHLYP/6-311+G**, PMP4/6-311+G(3df,2p)//BHLYP levels, the CVT/SCT rate constants based on the scaled potential energy curve at the PMP4/6-311+G (3df,2p)//BHLYP level, the TST and CVT rate constants at the PMP4/6-311+G (3df,2p)//BHLYP level, and the available experimental data *k* ($cm^3\ mol^{-1}\ s^{-1}$) vs 1000/*T* (K^{-1}) in the temperature range of 200−3000 K.

is to scale the computed potential energy curve. If one can tolerate the adjustment (the PMP4/6-311+G(3df,2p)//BHLYP potential energy scaled by 0.913), an excellent agreement of theoretical rate constant (6.50×10^{10}) with experiment (6.63×10^{10}) at 293 K can be found for the reaction, and the rate-constant results within 200−3000 K are also showed in the sixth column of Table 4. Accordingly, the reaction potential barrier is 5.47 kcal/mol based on the scaled potential energy curve. To clarify the main results in this paper, we plotted both theoretical and experimental[8] rate constants against 1000/*T* (K) in Figure 5. From comparisons of theoretical and experimental rate constants, it is found that the PMP4/6-311+G(3df,2p)//BHLYP and G2//QCISD methods are two reliable ones for the reaction, while the former processes an absolute advantage of calculation resource in comparison with the later. The reaction rate constants based on the scaled PMP4/6-311+G(3df,2p)//BHLYP potential

TABLE 5: Some Parameters for the Reactions of H Atoms with SiH_3F, SiH_3Cl, and SiH_4

	no. of Si−H bonds	*k*/*n* (10^{-13} $cm^3\ s^{-1}$)			*A*/*n* (10^{-11} $cm^3\ s^{-1}$)[b]		E_a ($kcal.mol^{-1}$)[b]		*D*(Si−H) ($kcal\ mol^{-1}$)	ΔH^0_{298} ($kcal\ mol^{-1}$)
		ref 24	ref 8	this work[a]	ref 24	this work	ref 24	this work		
$SiH_3F + H$	3		0.37	0.36		1.42		3.53	93.81	−9.98
$SiH_3Cl + H$	3	0.57		0.56	1.0	1.59	3.04	3.37	91.49	−12.30
$SiH_4 + H$	4	0.50	0.55	0.50	0.58	1.27	2.77	3.35	91.19	−12.58

[a] At 300 K for H atoms with SiH_3Cl and SiH_4; at 293 K for H atom with SiH_3F. [b] Within 293−490 K for $SiH_3F + H$, within 289−483 K for $SiH_3Cl + H$, and within 294−487 K for $SiH_4 + H$.

energy curve within 200−3000 K are fitted to be a three-parameter expression: $k = 3.3 \times 10^5 T^{2.60} \exp(-737/T)$ cm^3 mol^{-1} s^{-1} to describe the non-Arrhenius behavior of the rate constants within the broader temperature range.

D. Reactivity Trends. The effects of fluorine substitution and chlorine substitution on the reactivity of the Si−H bond in SiH_4 are evaluated by the present reaction systems of H atoms with SiH_3F, SiH_3Cl, and SiH_4, and some parameters are compared in Table 5 (this work, refs 1 and 2). To provide the most possible comparison with experiment, we presented for the data of "this work" the results based on the scaled MEP for the three reactions. The k/n is the value of room-temperature rate constant corrected for reaction-path degeneracy, A/n is the A-factor, similarly corrected, n is the number of Si−H bonds, and E_a is the reaction activation energy. From Table 5, one can see that the effect of chlorine substitution on the k/n value is small, but for fluorine substitution the effect is larger, which is consistent with the experimental results.[8,24] The small effect of chlorine substitution on k/n is primarily due to the small change of activation energy. But for fluorine substitution, there is a larger increase in activation energy, which results in the decrease in rate constant. Also from Table 5, we can see that fluorine substitution leads to a larger increase in the Si−H bond dissociation energy in comparison with chlorine substitution. The larger Si−H bond dissociation energy in SiH_3F will make the reaction more difficult to proceed. In addition, from SiH_3F to SiH_3Cl to SiH_4, the reaction will proceed with an "earlier" transition state, and this is the behavior expected from Hammond's postulate, since the reaction is more exothermic in the sequence.

Conclusions

In this paper, the hydrogen abstraction reaction: $SiH_3F + H \rightarrow SiH_2F + H_2$ has been investigated by ab initio and DFT direct dynamics methods. The changes of the bond lengths, generalized normal-mode vibrational frequencies, potential energies, and total curvature along MEP of the two methods are very similar. The results show that the BHLYP/6-311+G** method can provide accurate geometry and frequency information that are comparable to those from the UQCISD/6-311+G** method. In addition, the series of single-point calculations at the PMP4/6-311+G(3df,2p)//BHLYP and G2//QCISD levels are essential to improving the potential energy curve to obtain satisfactory reaction rate constants. The rate constants in the temperature range of 200−3000 K are calculated by the canonical variational transition-state theory with the small-curvature tunneling correction method. The CVT/SCT rate constant at the PMP4/6-311+G(3df,2p)//BHLYP level is in the best agreement with the experimental one among the four ab initio and DFT levels. The rate constant based on the scaled PMP4/6-311+G(3df,2p)//BHLYP potential energy curve is in the excellent agreement with the experimental value at 293 K, and the rate constants within 200−3000 K are fitted to be a three-parameter expression: $k = 3.3 \times 10^5 T^{2.60} \exp(-737/T)$ cm^3 mol^{-1} s^{-1}. The variational effect is small, and the small-curvature tunneling effect is important within the lower-temperature range. Fluorine substitution decreases the reactivity of the Si−H bond toward H atom attack, and the decrease in k/n mainly stems from a corresponding increase in activation energy.

Acknowledgment. Authors thank Professor Donald G. Truhlar for providing the POLYRATE-Version 8.4.1 program. This work is supported by the National Science Foundation of People's Republic of China (Project 29892168).

References and Notes

(1) Yu, X.; Li, S.-M.; Li, Z.-S.; Sun, C.-C. *J. Phys. Chem. A* **2000**, *104*, 9207.
(2) Li, S.-M.; Yu, X.; Xu, Z.-F.; Li, Z.-S.; Sun, C.-C. *J. Mol. Struct. (THEOCHEM)*, **2001**, *540*, 219.
(3) Koinuma, H.; Manako, T.; Natsuaki, H.; Fujioka H.; Fueki, K. *J. Non-Cryst. Solids* **1985**, *77*, 801.
(4) Matsuda, A.; Yagii, K.; Kaga, T.; Tanaka, K. *Jpn. J. Appl. Phys.* **1984**, *23*, 576.
(5) Sato, K.; Hirano, T.; Natsuaki, H.; Fueki, K.; Koinuma, H. *Appl. Phys. Lett.* **1984**, *45*, 1324.
(6) Schlegel, H. B. *J. Phys. Chem.* **1984**, *88*, 6254.
(7) Ho, P.; Melius, C. F. *J. Phys. Chem.* **1990**, *94*, 5120.
(8) Koshi, M.; Tamura, F.; Matsui, H. *Chem. Phys. Lett.* **1990**, *173*, 235.
(9) Truhlar, D. G.; Gordon, M. S. *Science* **1990**, *249*, 491.
(10) Duncan, W. T. Ph.D. Thesis, University of Utah, 1999.
(11) Duncan, W. T.; Truong, T. N. *J. Chem. Phys.* **1995**, *103*, 9642.
(12) Truong, T. N.; Duncan, W. T.; Bell, R. L. In *Chemical Applications of Density-Functional Theory*; American Chemical Society: Washington, DC, 1996; p 85.
(13) Truong, T. N. *J. Chem. Phys.* **1994**, *100*, 8014.
(14) Maity, D. K.; Duncan, W. T.; Truong, T. N. *J. Phys. Chem. A* **1999**, *103*, 2152.
(15) Frisch, M. J.; Trucks, G. W.; Schlegel, H. B.; Scuseria, G. E.; Robb, M. A.; Cheeseman, J. R.; Zakrzewski, V. G.; Montgomery, J. A., Jr.; Stratmann, R. E.; Burant, J. C.; Dapprich, S.; Millam, J. M.; Daniels, A. D.; Kudin, K. N.; Strain, M. C.; Farkas, O.; Tomasi, J.; Barone, V.; Cossi, M.; Cammi, R.; Mennucci, B.; Pomelli, C.; Adamo, C.; Clifford, S.; Ochterski, J.; Petersson, G. A.; Ayala, P. Y.; Cui, Q.; Morokuma, K.; Malick, D. K.; Rabuck, A. D.; Raghavachari, K.; Foresman, J. B.; Cioslowski, J.; Ortiz, J. V.; Baboul, A. G.; Stefanov, B. B.; Liu, G.; Liashenko, A.; Piskorz, P.; Komaromi, I.; Gomperts, R.; Martin, R. L.; Fox, D. J.; Keith, T.; Al-Laham, M. A.; Peng, C. Y.; Nanayakkara, A.; Gonzalez, C.; Challacombe, M.; Gill, P. M. W.; Johnson, B.; Chen, W.; Wong, M. W.; Andres, J. L.; Gonzalez, C.; Head-Gordon, M.; Replogle, E. S.; Pople, J. A. *Gaussian 98*; Gaussian, Inc.: Pittsburgh, PA, 1998.
(16) Durant, J. L., Jr.; Rohlfing, C. M. *J. Chem. Phys.* **1993**, *98*, 8031.
(17) Curtiss, L. A.; Raghavachari, L.; Trucks, G. W.; Pople, J. A. *J. Chem. Phys.* **1991**, *94*, 7221.
(18) Chuang, Y.-Y.; Corchado, J. C.; Fast, P. L.; Villa, J.; Hu, W.-P.; Liu, Y.-P.; Lynch, G. C.; Jackels, C. F.; Nguyen, K. A.; Gu, M. Z.; Rossi, I.; Coitino, E. L.; Clayton, S.; Melissas, V. S.; Lynch, B. J.; Steckler, R.; Garrett, B. C.; Isaacson, A. D.; Truhlar, D. G. *POLYRATE*, version 8.4.1; University of Minnesota: Minneapolis, MN, 2000.
(19) Truhlar, D. G.; Isaacson, A. D.; Garret, B. C. In *Theory of Chemical Reaction Dynamics*; Baer, M., Ed.; CRC Press: Boca Raton, FL, 1985; p 65.
(20) Steckler, R.; Hu, W.-P.; Liu, Y.-P.; Lynch, G. C.; Garrett, B. C.; Isaacson, A. D.; Melissas, V. S.; Lu, D.-H.; Troung, T. N.; Rai, S. N.; Hancock, G. C.; Lauderdale, J. G.; Joseph, T.; Truhlar, D. G. *Comput. Phys. Commun.* **1995**, *88*, 341.
(21) Lide, D. R., Ed. In *CRC Handbook of Chemistry and Physics*, 79th ed.; CRC Press: NewYork, 1998.
(22) Shimanouchi, T. *Tables of Molecular Vibrational Frequencies Consolidated Volume I*; National Bureau of Standards, U.S Government Printing Office: Washington, DC, 1972.
(23) Stull, D. R.; Prophet, H. *Natl. Stand. Ref. Data Ser., Natl. Bur. Stand.* **1971**, 37, and supplements.
(24) Arthur, N. L.; Potzinger, P.; Reimann, B.; Steenbergen, H.-P. *J. Chem. Soc., Faraday Trans. 2* **1989**, *85*, 1447.